NANO LETTERS

2004
Vol. 4, No. 6
1079−1083

Integration of Photosynthetic Protein Molecular Complexes in Solid-State Electronic Devices

Rupa Das,[†] Patrick J. Kiley,[†,‡] Michael Segal,[†] Julie Norville,[†] A. Amy Yu,[§] Leyu Wang,[||] Scott A. Trammell,[||] L. Evan Reddick,[⊥] Rajay Kumar,[†] Francesco Stellacci,[§] Nikolai Lebedev,[||] Joel Schnur,[||] Barry D. Bruce,[⊥,#] Shuguang Zhang,[‡,▼] and Marc Baldo*[,†]

Department of Electrical Engineering and Computer Science, Center for Biomedical Engineering, Department of Materials Science and Engineering, and Center for Bits and Atoms, Massachusetts Institute of Technology, Cambridge, Massachusetts 02139, Center for Bio/Molecular Science and Engineering, U.S. Naval Research Laboratory, Washington, D.C. 20375, and Department of Biochemistry, Cellular and Molecular Biology, and Center of Excellence in Environmental Biotechnology, University of Tennessee, Knoxville, Tennessee 37996

Received March 15, 2004; Revised Manuscript Received April 21, 2004

ABSTRACT

Plants and photosynthetic bacteria contain protein–molecular complexes that harvest photons with nearly optimum quantum yield and an expected power conversion efficiency exceeding 20%. In this work, we demonstrate the integration of electrically active photosynthetic protein–molecular complexes in solid-state devices, realizing photodetectors and photovoltaic cells with internal quantum efficiencies of approximately 12%. Electronic integration of devices is achieved by self-assembling an oriented monolayer of photosynthetic complexes, stabilizing them with surfactant peptides, and then coating them with a protective organic semiconductor.

Photosynthetic complexes are archetypal molecular electronic devices, containing molecular optical and electronic circuitry organized by a protein scaffold. Conventional technology cannot equal the density of the molecular circuitry found in photosynthetic complexes.[1] Thus, if integrated with solid-state electronics, photosynthetic complexes might offer an attractive architecture for future generations of circuitry where molecular components are organized by a macromolecular scaffold. But like other protein molecular complexes, photosynthetic complexes are soft materials, optimized for operation in a lipid bilayer interface between aqueous solutions. For utilization in practical technological devices they must be stabilized and integrated with solid-state electronics.

In this work, we demonstrate a technique for integrating photosynthetic complexes with solid-state electronics. The generality of the technology is demonstrated by its application to two types of photosynthetic complexes. The simplest, and more robust, photosynthetic complex used is a bacterial reaction center (RC), isolated from the purple bacterium *Rhodobacter (Rb.) sphaeroides*. This RC consists of three protein subunits[2] labeled L, M, and H, that together coordinate six pigment molecules: a bacteriochlorophyll dimer known as the special pair, P, two monomer bacteriochlorophylls, B_L and B_M, two bacteriopheophytins, H_L and H_M, and two quinones, Q_a and Q_b. These molecules are symmetrically arranged in the L and M subunits,[2] but electron transfer is observed to occur principally through the L branch, and the quinone Q_b is the ultimate electron acceptor in the complex.[3] In addition to the *Rb. sphaeroides* RC, we also employ a much larger complex, Photosystem I (PSI), which is isolated here from spinach chloroplasts. Although its core is similar to the more primitive RC, PSI contains up to fourteen subunits.[4] Together with its associated light harvesting complexes, PSI coordinates approximately 200 chlorophyll molecules.[5] PSI also contains three Fe_4S_4 complexes that act as the terminal electron acceptors and reside outside of the transmembrane domain of the PSI complex.[5]

Two key technologies are employed to preserve the functionality of these photosynthetic complexes outside their

* Corresponding author. E-mail: baldo@mit.edu
[†] Department of Electrical Engineering and Computer Science, MIT.
[‡] Center for Biomedical Engineering, MIT.
[§] Department of Materials Science and Engineering, MIT.
[▼] Center for Bits and Atoms, MIT.
[||] U.S. Naval Research Laboratory.
[⊥] Department of Biochemistry, Cellular and Molecular Biology, UT.
[#] Center of Excellence in Environmental Biotechnology, UT.

10.1021/nl049579f CCC: $27.50
Published on Web 05/19/2004

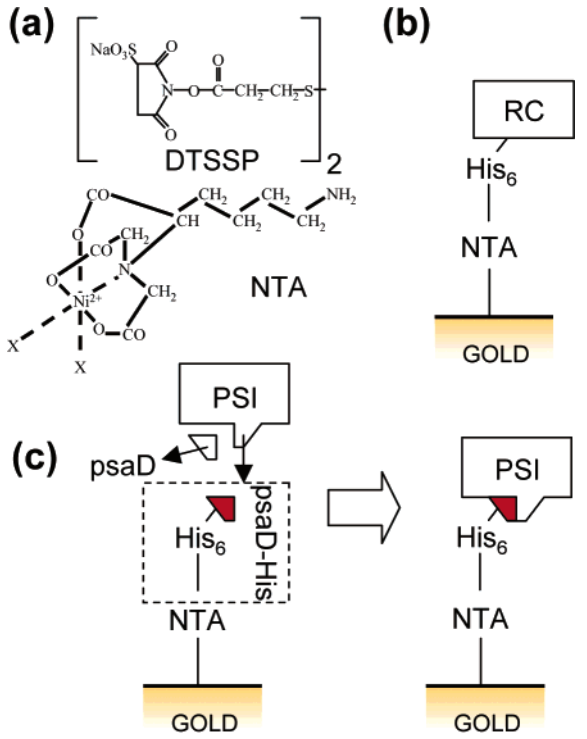

Figure 1. Techniques for oriented assembly of photosynthetic protein−molecular complexes. (a) To self-assemble oriented photosynthetic protein−molecular complexes, gold surfaces are first functionalized with DTSSP and then Ni^{2+}−NTA. (b) Bacterial reaction centers are immobilized using a His_6 tag at the C-terminal end of the M subunit. (c) Oriented PSI assembly is achieved when native psaD is exchanged with immobilized psaD-His, previously genetically modified with a His_6 tag.

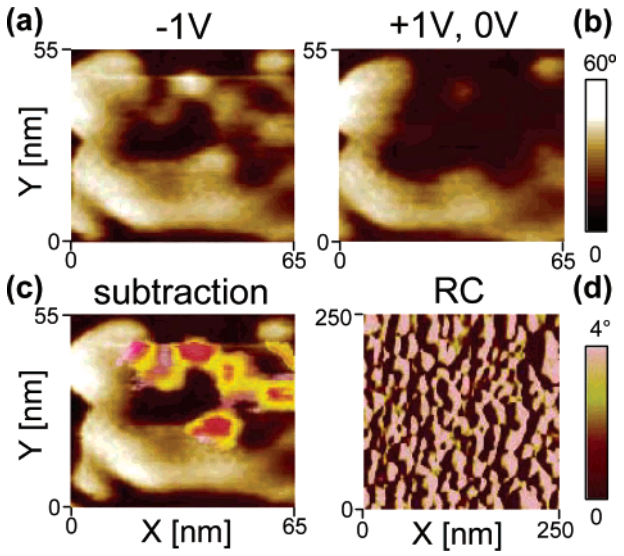

Figure 2. Characterization of self-assembled photosynthetic complexes by atomic force microscopy (AFM). The voltage dependence of a phase image of PSI particles is determined by applying a potential to the AFM tip. Note the phase changes in (a) the −1 V scan, relative to (b) the +1 V and 0 V scans. (c) Potential PSI particles are highlighted by superimposing a subtraction of the two images in (a) and (b) onto the −1 V scan. The voltage dependence confirms that the rectifying PSI complexes are oriented with the P700 dimer face up. (d) The phase profile of an assembled RC film showing a close-packed monolayer.

native environment. To stabilize the photosynthetic complexes during device fabrication, we add two peptide surfactants, one cationic A_6K (AAAAAAK), and the other anionic V_6D (VVVVVVD).[6−9] Then we deposit a thin (<1000 Å) layer of an amorphous organic semiconductor between the photosynthetic complexes and a top metal contact. The use of thin films of organic semiconductors is established in photovoltaic applications[10] and they may be employed as solid-state antennae for photosynthetic complexes, thereby enhancing optical absorption.

Fabrication of devices proceeds as follows. Transparent and conductive indium−tin oxide (ITO)-coated glass[11] is used as the substrate for all photosensitive devices. A self-assembled monolayer of Ni^{2+}−NTA on ITO is used to orient photosynthetic components by selectively binding polyhistidine tags present on each complex;[12] see Figure 1. To facilitate chemical functionalization of the ITO surface, a thin, discontinuous 4 nm-thick film of gold is thermally evaporated on the ITO using a 1 nm-thick layer of Cr to promote adhesion. NTA functionalization of ITO/Au proceeds by first incubating with 6.1 mg/mL DTSSP for 10 min,[13] then after washing with deionized H_2O, incubating the surface with 0.33 mg/mL NTA ligand for 10 min.[14] Finally, the NTA-functionalized surface is charged with 200 mM nickel sulfate; see Figure 1a. Polyhistidine-tagged RCs are expressed and isolated from *Rb. sphaeroides* strain SMpHis with the tag constructed at the C-terminal end of the RC M-subunit.[15] The expression and purification procedure was performed as described earlier.[16] RCs are then immobilized by incubating the functionalized ITO surface with approximately 100 μL of RC solution (0.2 mg/mL in 10 mM phosphate buffer pH 7.4, 0.05% LDAO and 0.02 M A_6K/V_6D (1:1)) for 1 h at 4 °C in the dark; see Figure 1b.

Native PSI complexes are isolated from spinach leaves as described earlier.[17] A single His_6 tag is introduced to isolated PSI complexes by engineering a protein subunit of PSI, psaD; see Figure 1c. First, the gene psaD from *Prochlorococcus marinus* is cloned into pET-21b between NdeI and XhoI, adding a C-terminal His_6 tag.[18] This recombinant psaD-His protein was expressed in *E. coli* (BL21 [DE3]) and purified by immobilized metal affinity chromatography. Next, the genetically modified protein (psaD-His) is immobilized on the Ni^{2+}−NTA functionalized ITO/Au surface and the unbound protein removed by washing. Finally, the surface is incubated with native PSI in 50 mM Tris, 25 mM NaCl, 2 M sucrose, 0.02% Triton X-100, and 0.02 M A_6K/V_6D (1:1) for 1 h at 4 °C in the dark. This incubation permits the intrinsic psaD subunit to be exchanged from the native PSI complexes and replaced by the immobilized psaD-His,[19] thereby immobilizing the PSI with its special pair oriented away from the ITO/Au substrate; see Figure 1d. It is believed that a similar exchange process occurs in vivo, allowing plants to replace photodamaged psaD.[19]

Tapping mode atomic force microscopy (TM-AFM) images of RC and PSI self-assembled monolayers on atomically flat Au-on-mica substrates are shown in Figure 2. To confirm the orientation of the PSI complexes we performed TM-AFM phase imaging in the intermittent contact mode and varied

the potential between the AFM tip and the ITO/Au substrate. The phase angle of the driven vibration of the cantilever in TM-AFM is related to the energy dissipated in the tip−sample interaction.[20] Thus, phase images of biological materials provide a map of the dissipative part of the sample's mechanical response. When a potential is applied to the AFM tip, we can alter its mechanical interactions with polar or charged samples by, for example, aligning polar molecules in the electric field. Voltage-dependent phase scans of a typical region of an assembled film are shown in Figure 2a and b. Phase scans taken at +1 V and 0 V show little difference, but phase scans taken at −1 V exhibit the appearance of localized regions of increased phase. A subtraction of the −1 V and 0 V images is superimposed on the −1 V image in Figure 2c. The increase in phase in the −1 V scan corresponds to an increase in the attractive forces between the tip and the sample[20] and indicates the presence of a positive charge trapped on the surface of PSI, mostly likely at the special pair, P700. Thus, the voltage dependence of TM-AFM phase imaging is consistent with the expected rectifying characteristics[21] of PSI in the orientation prescribed by self-assembly via exchange of psaD. PSI films formed using this method are less densely packed than the film of RC particles shown in Figure 2d.

The structures of the PSI and RC-based devices are shown in Figures 3a and b, respectively. To protect monolayers of PSI assembled on functionalized ITO we deposit via thermal evaporation at 10^{-6} Torr a thin coating of the archetype organic semiconductor tris(8-hydroxyquinoline) aluminum, Alq_3.[22] Alq_3 is transparent at the characteristic $\lambda = 680$ nm absorption peak of PSI. Alq_3 is also a preferentially electron-transporting material, thus under optical excitation at $\lambda = 680$ nm, charges are generated primarily in PSI; electrons are transferred to the ITO substrate, holes are trapped on the special pair, P700, and the device acts as a photodetector. Fabrication of PSI-based devices is completed by deposition at 10^{-6} Torr of a 80-nm-thick film of Al deposited through a 1-mm-diameter shadow mask.

Owing to the topology of their respective polyhistidine tags, PSI and RC complexes are immobilized on the Ni^{2+}−NTA in opposite orientations. RCs are oriented with their electron-accepting special pair, P, facing the substrate. The RC-based photovoltaic cell shown in Figure 3b employs a 60 nm-thick protective layer of the preferentially electron transporting fullerene C60. C60 was chosen because of its relatively deep lowest unoccupied molecular orbital (LUMO) energy of 4.7 eV[23] that could enhance electron transfer from the electron acceptor Q_b in the RC. After C60, a 12 nm-thick layer of 2,9-dimethyl-4,7-diphenyl-1,10-phenanthroline (bathocuproine, or BCP)[22] is deposited. The thin BCP layer is damaged by subsequent deposition of an 80 nm thick Ag cathode through a 1 mm diameter shadow mask. Damage to BCP facilitates electron extraction[24] and the deep highest occupied molecular orbital (HOMO) of BCP effectively prevents the injection of holes into the device, markedly improving the device's reverse bias characteristics. Thermally evaporated films of C60, BCP, and Ag were deposited at a rate of ≈ 0.3 nm/s in a vacuum of < 10^{-6} Torr.

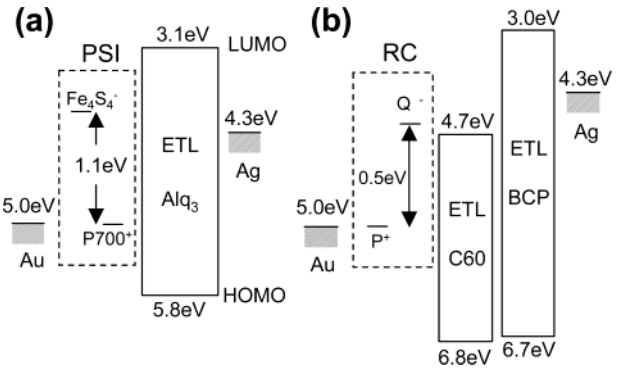

Figure 3. (a) Energy level diagram of a PSI photodetector. The highest occupied molecular orbital (HOMO) energy of the electron transport layer (ETL) Alq_3 is given by its ionization potential, extracted from ref 22. The relative $P700^+$ and $Fe_4S_4^-$ energy levels are taken from ref 1. (b) Energy level diagram of an RC photovoltaic cell. HOMO energies of the ETL's C60 and BCP are from refs 23 and 22, respectively. The relative P^+ and Q^- energy levels are taken from ref 1. Lowest unoccupied molecular orbital (LUMO) energies are estimated from the HOMO and the optical energy gap. It is assumed that no charge transfer occurs at the material interfaces.

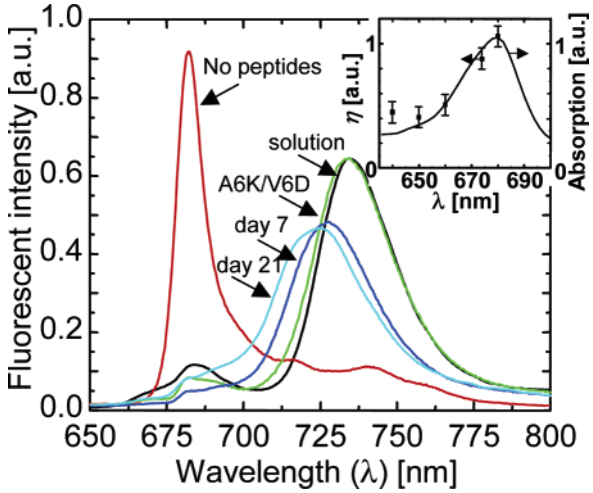

Figure 4. Comparison between the fluorescence spectrum of frozen ($T = 10$ K) PSI solution as extracted from spinach, with washed and dried films of PSI, demonstrates that PSI may be protected against degradation after washing and drying steps by stabilizing the complex with the surfactant peptides A_6K and V_6D. The stabilizing action of A_6K/V_6D is preserved for several weeks for dried films left in ambient conditions. (Inset) the stabilized PSI devices of Figure 3a exhibit a photocurrent spectrum that matches the absorption spectrum, confirming solid-state integration of stabilized PSI.

During device fabrication self-assembled monolayers of photosynthetic complexes must survive both a washing step, to remove surplus nonspecifically bound materials, and a drying step, to prepare the substrate for deposition of the semiconducting protective coating. The complexity and size of PSI makes it especially sensitive to degradation and dissociation.[25,26] The stability of PSI is assessed in Figure 4 using its fluorescent spectrum, which is enhanced at low temperatures. Thick, vacuum-dried films of PSI prepared without substrate functionalization were exposed to a pump laser at $\lambda = 408$ nm with intensity 0.5 mW/cm^2. At $T = 20$ K, in the absence of the stabilizing surfactant peptides, dried

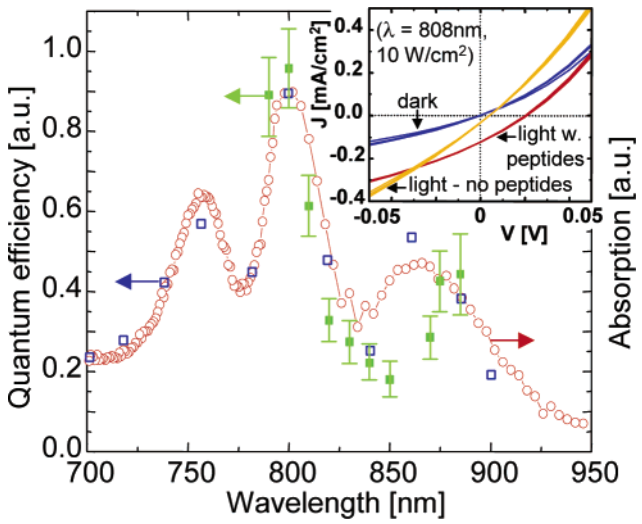

Figure 5. Photocurrent spectrum of photovoltaic devices employing bacterial reaction centers. A comparison between the photocurrent spectrum of solid-state (■) and wet electrochemical cell devices (□) and the solution absorption spectrum of the bacterial reaction centers (○), demonstrates that the observed photocurrent originates in the RCs. Wet cell device data is from ref 16. (Inset) stabilization of RC complexes with A_6K/V_6D peptides improves the internal quantum efficiency of the devices to 12% under short circuit conditions.

films of native PSI diluted in buffer exhibited significantly degraded fluorescence at $\lambda \approx 735$ nm. Polyelectrolytes such as poly(ethylene glycol), which may be used to preserve dried biological materials,[27] were similarly ineffective. In contrast, incubating PSI with A_6K/V_6D was found to almost entirely preserve the low-temperature fluorescent spectrum of PSI. The $\lambda = 735$ nm fluorescent peak of peptide-stabilized films stored in an ambient environment exhibited a gradual blue shift over several weeks, indicative of gradual structural changes in the light harvesting antennae of PSI.[28] In the inset of Figure 4, we show that the photocurrent spectrum of PSI−A_6K/V_6D devices exhibits the $\lambda = 680$ nm peak characteristic of the absorption spectrum of PSI, which, in conjunction with the low-temperature fluorescent data, demonstrates that PSI has been successfully integrated in a solid-state environment.

Unlike PSI, the activity of a significant fraction of the more robust RC complexes can be preserved, even in the absence of peptide surfactants. In Figure 5, the activity of an RC-based device without A_6K or V_6D is confirmed by spectrally resolving the short circuit current using a Ti−sapphire CW laser tunable between $\lambda = 790$ nm and $\lambda = 890$ nm. The photocurrent spectrum exhibits the characteristic peaks of both the solution absorption spectrum of the RC complexes, and a photocurrent spectrum of identical RC complexes in an electrochemical cell reproduced from ref 16. In the inset, we show the effect of A_6K/V_6D stabilization on the current−voltage characteristics of the devices. On average, the peptides were found to improve the open circuit voltage by a factor of 2−3.

The short circuit current density of the RC−A_6K/V_6D devices is 0.12 mA/cm^2 under an excitation intensity of 10 W/cm^2 at $\lambda = 808$ nm. Assuming a perfectly formed RC monolayer of density 3×10^{-12} mol/cm^2, and given an extinction coefficient of 2.9×10^5 M^{-1} cm^{-1},[29] we calculate the optimum photocurrent as 1 mA/cm^2, where we have ignored possible microcavity effects due to reflections from the ITO/Au electrode and assumed 100% reflection of the optical pump by the Ag cathode. Thus, under short-circuit conditions, a conservative estimate of the internal quantum efficiency of the device is 12%.

In conclusion, our results suggest that photosynthetic complexes may be used as an interfacial material in photovoltaic devices. Evolved within a thin membrane interface, photosynthetic complexes sustain large open circuit voltages of 1.1V[1] without significant electron−hole recombination, and they may be self-assembled into an insulating membrane, further reducing recombination losses. We have demonstrated here that they may be integrated in solid-state devices. Peptide surfactants have proved essential in stabilizing these complexes during and after device fabrication. Given typical quantum yields for photoinduced charge generation[1] of > 95% it is expected that the power conversion efficiency of a peptide-stabilized solid-state photosynthetic device may approach or exceed 20%. Similar integration techniques may applied to other biological or synthetic protein−molecular complexes.

Acknowledgment. The authors are grateful for discussions with Peter Peumans, and Elizabeth Broadwater for sample preparation. This work was funded by DARPA and AFOSR under contract F49620-02-1-0399 and in part by the MRSEC Program of the NSF under award DMR 02-13282. S.Z. acknowledges funding by MURI/AFOSR. Part of the data was taken with the assistance of Joe Gardecki using Laser Biomedical Research Center facilities supported by NIH grant P41 RR 02594 and Laser Research Facility supported by NSF grant 011137 CHE. Travel of B.D. Bruce was facilitated by a SARIF grant from UTK. Das and Kiley contributed equally to this work.

References

(1) Hoff, A. J.; Deisenhofer, J. *Phys. Rep.* **1997**, *287*, 1−247.
(2) Allen, J. P.; Feher, G.; Yeates, T. O.; Rees, D. C.; Deisenhoffer, J.; Michel, H.; Huber, R. *Proc. Nat. Acad. Sci. U.S.A.* **1986**, *83*, 8589−8593.
(3) Hörber, J. K. H.; Göbel, W.; Ogrodnik, A.; Michel-Beyerle, M. E.; Cogdell, R. J. *FEBS Lett.* **1986**, *198*, 268−272.
(4) Chitnis, P. R. *Annu. Rev. Plant Phys. Plant Mol. Biol.* **2001**, *52*.
(5) Ben-Shen, A.; Frolow, F.; Nelson, N. *Nature* **2003**, *426*, 630−635.
(6) Vauthey, S.; Santoso, S.; Gong, H.; Watson, N.; Zhang, S. *Proc. Natl. Acad. Sci. U.S.A.* **2002**, *99*, 5355−5360.
(7) Santoso, S.; Hwang, W.; Hartman, H.; Zhang, S. *Nano Lett.* **2002**, *2*, 687−691.
(8) von Maltzahn, G.; Vauthey, S.; Santoso, S.; Zhang, S. *Langmuir* **2003**, *19*, 4332−4337.
(9) Zhang, S. *Nature Biotechnol.* **2003**, *21*, 1171−1178.
(10) Tang, C. W. *Appl. Phys. Lett.* **1985**, *48*, 183−185.
(11) Applied Films, Boulder, Colorado.
(12) Smith, M. C.; Furman, T. C.; Ingolia, T. D.; Pidgeon, C. *J. Biol. Chem.* **1988**, *263*, 7211−7215.
(13) Katz, E. Y. *J. Electro. Chem.* **1990**, *291*, 257−260.
(14) Dithiobis(sulphosuccinimidyl propionate) (DTSSP) is obtained from Pierce Biotechnology, Rockford, IL. Nitrilotriacetic acid (NTA) ligand is obtained from Qiagen Inc., Valencia, CA.
(15) Goldsmith, J. O.; Boxer, S. G. *Biochim. Biophys. Acta* **1996**, *1276*, 171−175.
(16) Trammell, S. A.; Wang, L.; Zullo, J. M.; Shashidhar, R.; Lebedev, N. *Biosens. Bioelectron.* **2004**, *19*, 1649−1655.

(17) Bruce, B. D.; Malkin, R. *J. Biol. Chem.* **1988**, *263*, 7302−7308.
(18) pET-21B was obtained from Novagen, Madison, WI.
(19) Minai, L.; Fish, A.; Darash-Yahana, M.; Verchovsky, L.; Nechushtai, R. *Biochemistry* **2001**, *40*, 12754−12760.
(20) Cleveland, J. P.; Anczykowski, B.; Schmid, A. E.; Elings, V. B. *Appl. Phys. Lett.* **1998**, *72*, 2613−2615.
(21) Lee, I.; Lee, J. W.; Greenbaum, E. *Phys. Rev. Lett.* **1997**, *79*, 3294−3297.
(22) Hill, I. G.; Kahn, A. *J. Appl. Phys.* **1999**, *86*, 4515−4519.
(23) Dutton, G.; Zhou, X.-Y. *J. Phys. Chem. B* **2002**, *106*, 5975−5981.
(24) Peumans, P.; Forrest, S. *Appl. Phys. Lett.* **2001**, *79*, 126−128.
(25) Croce, R.; Zucchelli, G.; Garlaschi, F. M.; Bassi, R.; Jennings, R. C. *Biochemistry* **1996**, *35*, 8572−8579.
(26) Nechushtai, R.; Nourizadeh, S. D.; Thornber, J. P. *Biochim. Biophys. Acta* **1986**, *848*, 193−200.
(27) Mi, Y. L.; Wood, G.; Thoma, L.; Rashed, S. *PDA J. Pharm. Sci. Technol.* **2002**, *56*, 115−123.
(28) Morosinotto, T.; Breton, J.; Bassi, R.; Croce, R. *J. Biol. Chem.* **2003**, *278*, 49223−49229.
(29) Straley, S. C.; Parson, W. W.; Mauzerall, D. C.; Clayton, R. K. *Biochim. Biophys. Acta* **1973**, *305*, 597−609.

NL049579F